HiSST: 2nd International Conference on High-Speed Vehicle Science & Technology

11–15 September 2022, Bruges, Belgium

Linearly-Combined Transition Model based on Empirical Spot Growth Correlations

Maximilian Karsch[1], *Jeroen Van den Eynde*[2] *& Johan Steelant*[3]

Abstract

The transition from laminar to turbulent flow in a hypersonic boundary layer is modelled using an intermittency-based linear combination approach. A simplified transition model like this enables a quick assessment of aero-thermal loads and the overall flight efficiency of high-speed vehicles during the initial design phase by weighting purely laminar and turbulent flow results on the basis of an empirically calculated intermittency. The transition model presented within this work includes an empirical model to account for Mach number, Reynolds number, wall temperature and pressure gradient effects on turbulent spot growth based on available turbulent spot studies in literature. A validation of the transition model is carried out for a number of different test cases and a methodology to extend the model to generic geometries is presented to enable a more general application.

Keywords: *high-speed transition modelling, turbulent spot growth, compressibility, wall temperature*

Nomenclature

Latin
C – Chapman-Rubesin parameter
K – Pressure gradient parameter
M – Mach number
r – Recovery factor
Re – Reynolds number
s – Spatial coordinate along streamline
St – Stanton number
T – Temperature
Tu – Turbulence level
u – Streamwise velocity
x – Spatial streamwise coordinate

Greek
β – Lateral spot spreading half-angle
γ – Intermittency
κ – Ratio of specific heats
μ – Dynamic viscosity
ν – Kinematic viscosity
$\hat{n}\sigma$ – Spot production parameter
θ – Momentum thickness
ρ – Density

Superscripts
$\star$ – Reference temperature

Subscripts
0 – Reference value
∞ – Free-stream condition
aw – Adiabatic wall
c – Convective
e – Boundary layer edge
jet – Lateral jet location
lam – Laminar
LE – Leading edge
t – Transitional
TE – Trailing edge
$turb$ – Turbulent
u – Unit value
w – Wall condition

1. Introduction

The process of laminar to turbulent boundary layer transition has important implications on the aerodynamic behaviour, the structural heating and the overall flight efficiency of high-speed vehicles. Although being studied for over a century, the concept of boundary layer transition is not fully understood and a universal method to accurately predict both onset and extent of transition is not available.

[1] *M.Sc. Aerospace Engineering, University of Stuttgart, max.karsch94@web.de*
[2] *Flight Vehicles & Aerothermodynamics Engineer, ESA/ESTEC, Jeroen.Van.den.Eynde@esa.int*
[3] *Senior Flight Vehicles & Aerothermodynamics Engineer, ESA/ESTEC, Johan.Steelant@esa.int*

To avoid dealing with transition or to apply a conservative approach, one may think of assuming a fully turbulent boundary layer on the whole vehicle to calculate the occurring aero-thermal loads. However, this would lead to much heavier vehicle concepts, compromising the maximum available payload significantly. An illustration of this matter was given in the context of the NASP program where a relative payload increase of 60% to 70% compared to the fully turbulent condition was estimated [1]. Likewise, it was also found that the vehicle take-off weight can vary by a factor of two or more depending on the estimated transition location [2]. The latter involves another popular engineering approach namely to estimate a fixed transition location based on empirical correlations and use turbulent calculations downstream. This disregards the finite extent of the transitional region and also implies a discontinuous distribution of the heat transfer coefficient as the boundary layer switches from laminar to turbulent instantaneously. Both approaches were found to be unsatisfactory, in particular with respect to hypersonic flight where the laminar flow region as well as the transition zone itself can be quite extensive and may occupy large portions of the vehicle. Starting at the transition onset location, the rate and consequently, the extent of the transitional region itself is governed by the individual growth and merger of turbulent spots.

Several transition models have been proposed in the past where the most promising ones include the concept of intermittency, a field variable which essentially describes the time fraction of the flow being turbulent at a certain location within the transitional zone. According to Narasimha [3], these models may be classified into the following four types based on their level of complexity: (a) Integral methods, (b) Algebraic models, (c) Differential equation models and (d) Direct methods. An overview of early transition models according to this classification was given by Narasimha & Dey [4].

The first and simplest class is described by integral methods in which the currently proposed linearly-combined model belongs to. Introduced by Emmons [5], the underlying idea is that laminar and turbulent flow are calculated independently from each other, e.g. by using two separate sets of Reynolds-averaged Navier-Stokes (RANS) equations. The mean flow within the transitional region is then reconstructed by blending purely laminar and turbulent flow components using the intermittency as a weighting parameter. In this context, the intermittency factor itself is typically determined by a simple analytical expression. Transition models of this type have been proposed by Dhawan & Narasimha [6], Solomon et al. [7] and Chen & Thyson [8]. Algebraic transition models use a single set of RANS equations but use an intermittency-scaled eddy viscosity to model a gradual release of turbulence throughout the transition region. Examples for transition models of this class are given by Adams [9] who used an analytical expression for the intermittency distribution and Cebeci & Smith [10].

Higher level transition models typically introduce an additional differential equation describing the intermittency transport. Steelant & Dick [11, 12, 13] used the concept of conditional averaging to derive two sets of equations, one for the laminar and one for the turbulent part of the flow which are coupled through the intermittency. Within this approach, laminar-turbulent interactions are included, however, the computational effort is effectively doubled. Therefore, efforts were made, e.g. by Simon & Stephens [14], Suzen & Huang [15] and Cho & Chung [16] to combine the two sets of equations into a single RANS equation set. Another pressing issue was the usage of integral boundary layer parameters in the models which are not locally accessible. Langtry & Menter addressed these aspects in their γ-$Re_{\theta t}$ transition model [17, 18] by introducing two transport equations for the intermittency and the transition onset Reynolds number based on local flow variables. These are solved together with a single set of RANS equations and a modified version of the SST k - ω turbulence model. The recently proposed γ-α transition model by Van den Eynde & Steelant [19, 20] uses a similar approach but includes mechanisms of turbulent spot growth to model the intermittency production and is completely decoupled from the applied turbulence model. It has shown promising potential in predicting hypersonic boundary layer transition with and without pressure gradients. Direct numerical simulations (DNS) are inherently capable of calculating transitional flow as the full Navier-Stokes equations are considered, however, the large computational effort needed to resolve the smaller scales of the flow make them unfeasible for most practical engineering applications. Nevertheless, direct methods are often used to investigate detailed features of the transition process, e.g. the growth and propagation of a single turbulent spot.

In this work, boundary layer transition is modelled by using a simple linear combination approach. Similar to the γ- and γ-α model [11, 12, 13, 19, 20], the aim is to incorporate mechanisms of turbulent spot growth to reconstruct the intermittency evolution throughout the transitional region. Therefore, empirical correlations are presented that aim to reproduce the effects of compressibility, temperature and Reynolds number on the propagation and growth of individual turbulent spots. As these correlations describe the process of spot growth from a phenomenological point of view, they are thought to useful in a more general context as well, e.g. for high-level transition models that use an intermittency-based approach.

2. Empirical correlations for turbulent spot growth

As the production, growth and propagation of turbulent spots represent the key mechanisms after breakdown, they need to be reproduced accordingly in the transition model to accurately predict the transition zone extent. In a plan view, the geometry of an individual spot may be represented in a simplified manner by a downstream pointing triangle as shown in Fig. 1. The concept of concentrated breakdown which was established by Narasimha [21] states that turbulent spots are generated at a certain streamwise location Re_{xt}. After the initial generation phase, turbulent spots approximately grow in a linear fashion as they propagate downstream until they eventually merge and form a fully turbulent boundary layer. While the rear of the spot moves with a velocity of u_{TE}, the spot front travels at a higher velocity u_{LE} which causes the spot to grow in longitudinal direction. Further, the growth in lateral direction is typically described with the spreading angle β formed between the symmetry line and the wing tip of the spot.

2.1. Spot propagation velocities

The spot propagation velocities have been reported to be a function of the Reynolds number within several studies found in literature. For instance, Wygnanski et al. [22] observed a decrease of the trailing edge velocity from 62% to 50% of the free-stream velocity in their experiments if the Reynolds number at the spot inception location was increased from $Re_\theta \approx 230$ to $Re_\theta \approx 580$. On the other hand, the leading edge velocity remained constant at 89% of the free-stream velocity.

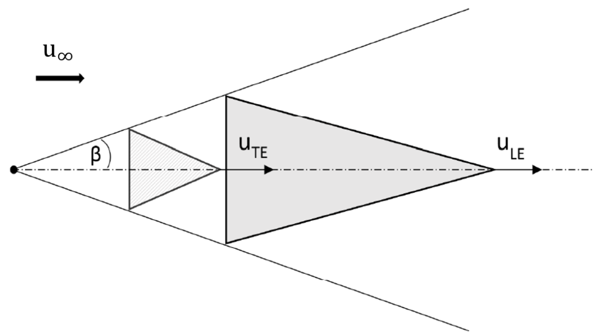

Fig 1. Turbulent spot geometry

In a numerical study, Johnson [23] also found inhibited spot growth at low Reynolds numbers which he attributed to the presence of strong viscous damping. Compared to the results of Wygnanski et al. [22] however, the decrease of the trailing edge velocity with increasing Reynolds number occurred more rapidly. Based on his obtained numerical results, Johnson also proposed correlations for the spot propagation velocities which are included in Fig. 2 for zero pressure gradient flow along with other spot data and the currently proposed correlations. As the decrease of the propagation velocities observed by Johnson was found to be too large, the correlations given in [23] for zero pressure gradient flow are modified to

$$\frac{u_{LE}}{u_e} = 0.15\,\text{exp}(-0.004\,Re_{\theta t}) + 0.85 \tag{1}$$

and

$$\frac{u_{TE}}{u_e} = 0.61\,\text{exp}(-0.005\,Re_{\theta t}) + 0.39 \qquad (2)$$

to obtain a better agreement with present experimental data although it is somewhat unclear which dataset is most representative. The used Reynolds number is defined based on the momentum thickness at the transition onset location according to the experimental and numerical data where the Reynolds number is typically specified at the spot inception point. Moreover, it is important to mention that measurements of spot propagation velocities are extremely sensitive with respect to the applied methodology. More precisely, a threshold criterion to define the turbulent/non-turbulent interface is required which differs among different spot studies. This is potentially a major cause of the scatter seen within the experimental and numerical data. In this context, a general convention to define the shape and extremities of turbulent spots is needed to enable a better comparison of spot growth data.

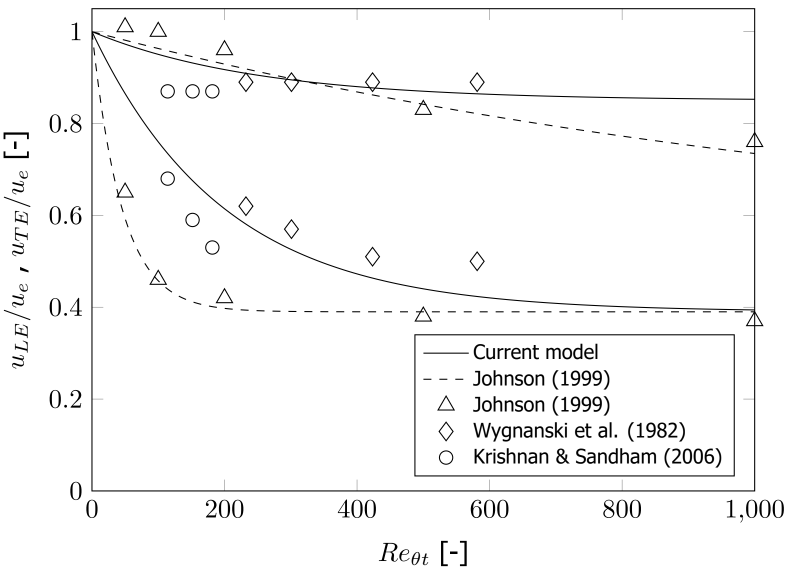

Fig 2. Spot propagation velocities

Apart from the scatter, the understanding of the full dependencies of the spot convection velocities is still incomplete and also requires further investigation. A number of studies, e.g. [23], [24] and [25], addressed the effect of favourable and adverse pressure gradients. In a recent work, Van den Eynde & Steelant [27] proposed an empirical correlation of the spot propagation velocities as a function of the Mach number.

2.2. Lateral spreading rate

Similar to the longitudinal spot growth, the lateral growth rate of turbulent spots has also been subject of several experimental and numerical studies in the past. A study by Fischer [28] who collected spreading rates of turbulent disturbances such as turbulent spots, wedges and jets revealed a strong Mach number effect on the lateral spreading resulting in a growth rate reduction by a factor of three at $M_\infty = 5$. This trend has been widely accepted and further confirmed with more recent results. However, quantifying this effect remains a challenge due to the scarcity of hypersonic results and the large scatter found in the data. Again, the latter is most likely related to different spot shape definitions. Further, experimental measurements by Chong & Zhong [29] on the three-dimensional structure of turbulent spots indicated the presence of a lateral overhang beneath the wing tip region of the spot. Based on this observation, consistently lower spreading angles should be expected for heat-transfer measurements at the wall compared to other measurement techniques such as hot-wire anemometry which are applied at a certain distance away from the wall. Regarding the driving mechanism behind the lateral growth, Gad-El-Hak [30] found that the lateral turbulence spreading principally occurs through a destabilization mechanism of the surrounding laminar boundary layer in addition to the classical turbulent entrainment mechanism. The mechanism was investigated in more detail within a numerical study by Redford et al. [31] which revealed the presence of lateral jets emanating from the wingtip region of the spots. This observation motivated Sandham [32] to formulate a convective Mach number for the lateral growth of turbulent spots in analogy to the growth rate of turbulent mixing layers as

$$M_c = M_e \frac{1 - u_{jet}/u_e}{1 + \sqrt{T_{jet}/T_e}} \tag{3}$$

where the subscript $(\cdot)_{jet}$ denotes the corresponding variable taken at the lateral jet location. The convective Mach number is used in the current work to encompass Mach number and temperature effects on turbulent spot growth within the transition model. While the streamwise velocity at the jet location is estimated with $u_{jet} \approx 0.45\, u_e$, the temperature ratio is approximated using the modified Crocco-Busemann relation

$$\frac{T_{jet}}{T_e} = 0.45 + 0.55\,\frac{T_w}{T_e} + 0.25\, r\, \frac{\kappa - 1}{2} M_e^2 \tag{4}$$

with the recovery factor r. The temperature effect on spot growth has been addressed in numerical studies, e.g. by Redford et al. [31] and Jocksch & Kleiser [33]. Overall, it was shown that the wall temperature plays a secondary role and that a cooled wall generally yields lower spreading angles.

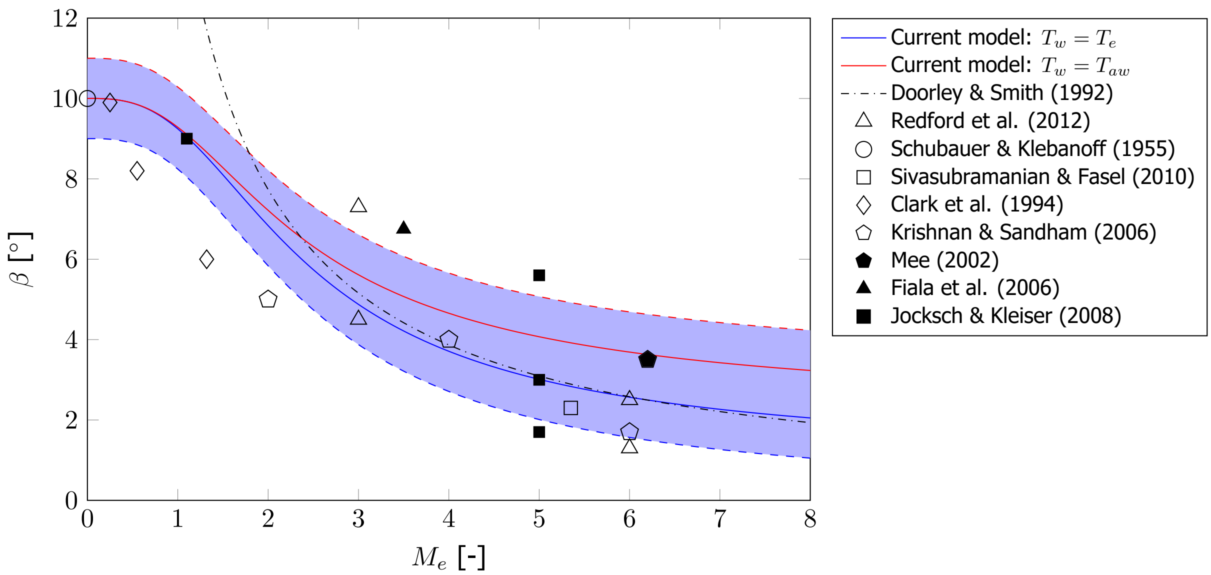

Fig 3. Lateral spot spreading angle

Besides the Mach number and temperature effect, the spreading angle is also reported to be a weak function of the Reynolds number, e.g. by Schubauer & Klebanoff [34] or Wygnanski et al. [22] with a slight reduction of β at lower Reynolds numbers. On the other hand, a numerical study by Jocksch & Kleiser [33] indicated a much stronger effect of the Reynolds number. Within the current model, the Reynolds number dependency is represented using a damping factor proposed by Johnson [23]. Regarding the convective Mach number dependency, an analytic function was fitted to the data given in [32] which in turn was obtained from linear stability theory. All in all, the current correlation for the lateral spot spreading angle reads

$$\frac{\beta}{\beta_0} = f_1(M_c)\, f_2(Re_{\theta t}) = \left(1 + 7.06\, M_c^{2.86}\right)^{-0.5} \left[1 - 0.29\, \text{exp}(-0.0035\, Re_{\theta t})\right] \tag{5}$$

where the incompressible reference value is $\beta_0 = 10°$ based on experimental results by Schubauer & Klebanoff [34]. The result for two different wall temperature conditions are plotted in Fig. 3 together with experimental and numerical results. Note that in this plot, the Reynolds number dependency is neglected, i.e. function f_2 from (5) is set to one. Within the current formulation, the stabilizing effect with respect to compressibility and wall cooling seems to be captured correctly. Additionally, it is interesting to note that the cold wall case is in quite good agreement with the theoretical model by Doorley & Smith [35] especially for $M_e > 5$. Given the model formulation of the spreading angle, one could argue that a more meaningful representation could be obtained by plotting directly over the convective Mach number rather than the edge Mach number. However, with the large scatter present in the dataset the trends are not clearly visible and no satisfactory collapse of the data could be achieved. A similar conclusion was drawn in a recent work by Van den Eynde & Steelant [27].

3. Methodology

The classical linear combination approach poses one of the simplest methods to model boundary layer transition and was found to provide an excellent description of the transition zone for two-dimensional flows with zero pressure gradient [3]. In essence, the underlying hypothesis of this model states that laminar and turbulent flow components do not interact by any means and develop independently. Using Narasimha's near-wall intermittency distribution, the purely laminar and turbulent flow components are combined in a linear fashion with their corresponding portions through

$$St = (1-\gamma)\, St_{lam} + \gamma\, St_{turb} \tag{6}$$

to reconstruct a transitional Stanton number. The laminar and turbulent flow components are obtained from theoretical expressions or numerical solutions while the intermittency is defined by

$$\gamma = \begin{cases} 1 - \exp(-\hat{n}\sigma (Re_x - Re_{xt})^2) & , Re_x > Re_{xt} \\ 0 & , Re_x \leq Re_{xt} \end{cases} \tag{7}$$

with the dimensionless spot production parameter $\hat{n}\sigma$ and the transition onset Reynolds number Re_{xt}. Regarding the transition onset Reynolds number, a correlation by Steelant & Dick [13] is used in combination with a compressibility factor given in [3] to yield

$$Re_{xt} = (400\,094\, Tu_\infty^{-1.38} - 105\,254\, Tu_\infty^{-7/8})(1 + 0.38\, M_e^{0.6}) \tag{8}$$

where Tu_∞ denotes the free-stream turbulence level in percent. This is based on a correlation proposed by Mayle [36] with

$$Re_{\theta t} = 420\, Tu_\infty^{-0.69} \tag{9}$$

but introduces the effect of distributed breakdown. Following the model formulation used by Van den Eynde & Steelant [19], the dimensionless spot production parameter is calculated according to

$$\hat{n}\sigma = c_1\, (Tu_\infty)^{c_2}\, f_\sigma\, f_K\, f_\gamma \tag{10}$$

with $c_1 = 1.25 \cdot 10^{-11}$ and $c_2 = 7/4$ taken from Mayle [36]. Another choice regarding these constants is considered herein as well based on the observation by Narasimha [3] that the modified spot formation rate $N = \hat{n}\sigma Re_{\theta t}^3$ is independent of Tu_∞. This suggests that $c_2 = 2.07$ if $Re_{\theta t} \propto Tu_\infty^{-0.69}$ is assumed. Further, several correction factors f are included in order to represent different effects on the spot production parameter $\hat{n}\sigma$. The empirical correlations for the leading edge velocity, the trailing edge velocity and the lateral spreading angle of the turbulent spot are combined to yield the relative spot growth parameter with

$$f_\sigma = \frac{\sigma}{\sigma_0} = \frac{1}{\sigma_0}\left(\frac{u_e}{u_{TE}} - \frac{u_e}{u_{LE}}\right)\tan(\beta) \tag{11}$$

according to Vinod & Govindarajan [37]. The reference value of $\sigma_0 = 0.25$ is obtained by evaluating the corresponding correlations at $M_c = 0$ and $Re_{\theta t} \to \infty$ to ensure $f_\sigma \leq 1$. Unlike formulations within previous models, this approach establishes a direct link between the total spot production parameter $\hat{n}\sigma$ and the phenomenological description of the turbulent spot with its propagation parameters u_{LE}, u_{TE} and β.

To also account for streamwise pressure gradient effects, an additional correction factor from Steelant & Dick [11] is used which is defined by

$$f_K = \begin{cases} (474\,Tu_\infty^{-2.9})^{(1-\exp(2\cdot 10^6\,K))} & ,\ K < 0 \\ 10^{-3227\,K^{0.5985}} & ,\ K \geq 0 \end{cases} \tag{12}$$

where the pressure gradient parameter is calculated as

$$K = -\frac{\mu_\infty}{\rho_\infty^2\,u_\infty^3}|1 - M_\infty^2|\frac{dp}{ds} \tag{13}$$

and dp/ds denotes the pressure gradient along the streamline. The third correction factor f_γ incorporates the concept of distributed breakdown and is defined by

$$f_\gamma = \begin{cases} 1 - \exp(-1.735\tan(5.45\,\gamma_{mod} - 0.95375) - 2.2) & ,\ \gamma_{mod} < 0.45 \\ 1 & ,\ \gamma_{mod} \geq 0.45 \end{cases} \tag{14}$$

according to Steelant & Dick [38]. A slightly modified argument with $\gamma_{mod} = \gamma + 0.01$ is used herein to exclude negative values for f_γ in the vicinity of x_t which would result in a negative intermittency production. The purpose of this correction factor is to gradually ramp up the spot production parameter $\hat{n}\sigma$ during the initial stage of transition which should enable the model to provide more realistic results.

It is important to mention that the analytic intermittency distribution from Eq. (7) represents an integrated formulation, i.e. it is valid for a constant spot production parameter $\hat{n}\sigma$. To allow for varying spot production throughout the domain, e.g. due to a spatially changing wall temperature, the differential formulation

$$\frac{1}{1-\gamma}\frac{d\gamma}{dx} = B(x) \quad \text{with} \quad B(x) = 2\,\hat{n}\sigma\frac{u^2}{\nu^2}(x - x_{tr}) \tag{15}$$

given in [11] is employed which yields

$$\gamma = 1 - \exp(-\int_{x_{tr}}^{x} B(x)\,dx) \quad , \quad x > x_{tr} \tag{16}$$

for the intermittency distribution. Before applying the presented model to a number of test cases, it is instructive to first investigate the sensitivity of the transition model with respect to compressibility and temperature effects. Therefore, intermittency distributions calculated with Eq. (7) for different Mach numbers and wall temperature conditions are shown in Fig. 4. In order to display the effect on the intermittency evolution, $Re_x - Re_{xt}$ is treated as an independent variable and the free-stream turbulence level is set to an arbitrary value of $Tu_\infty = 0.5\%$. For the sake of simplicity, the Reynolds number effect in this figure is neglected, i.e. Eq. (1), (2) and (5) are evaluated at $Re_\theta \to \infty$ limit and a zero pressure gradient flow with $f_K = 1$ is assumed. Fig 4 (a) exhibits the effect of an increasing edge Mach number from three to five on the intermittency evolution. As the Mach number is increased, the transition rate decreases which in turn results in an extended transitional region. If the end of the transition is defined at $\gamma = 0.99$, this extent is quantified with $Re_{\Delta xt} = 1.6 \cdot 10^6$ at Mach three and $Re_{\Delta xt} = 2.04 \cdot 10^6$ at Mach five, respectively. Likewise, a similar effect is noticed for wall cooling as shown in Fig. 4 (b) for a constant Mach number of five. In this case, the transition zone increases from $Re_{\Delta xt} = 1.75 \cdot 10^6$ to $Re_{\Delta xt} = 2.04 \cdot 10^6$ if the wall temperature is decreased from the adiabatic wall temperature down to the boundary layer edge temperature.

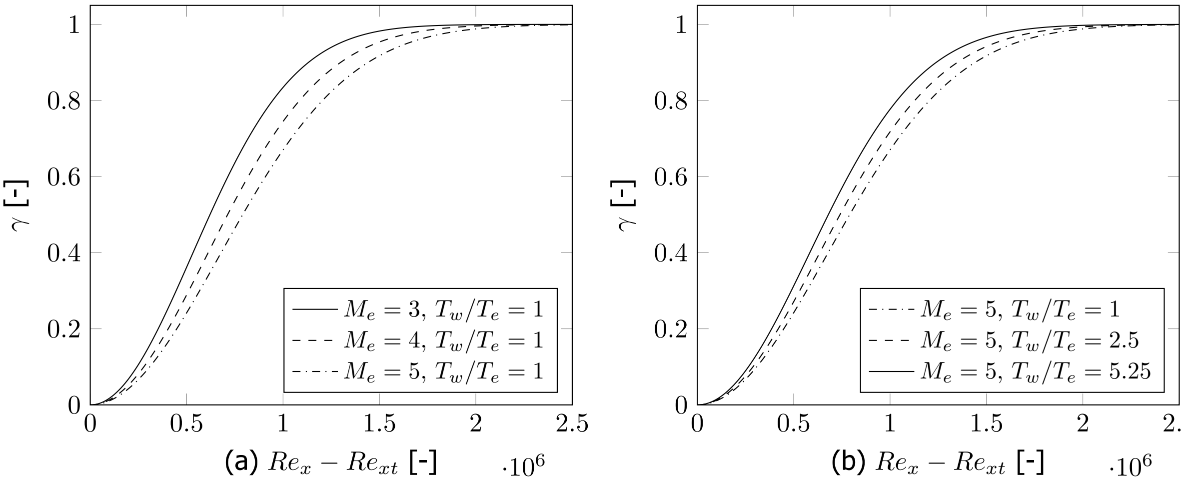

Fig 4. Sensitivity of intermittency distribution to Mach number and wall-to-edge temperature ratio

4. Validation

In the following, the proposed linearly-combined transition model is applied to several flat plate test cases which include both hot and cold wall temperature conditions as well as incompressible and hypersonic flow.

4.1. T3 series

Several incompressible boundary layer transition experiments with varying free-stream turbulence levels were carried out by Roach & Brierley [39] on a flat plate and are used herein for comparisons with the results provided by the linearly-combined transition model. The corresponding test conditions for the cases under consideration are summarized in Tab. 1.

Table 1. Test conditions of T3A and T3B case

Case	Tu_∞ [%]	u_∞ [m/s]	ρ_∞ [kg/m^3]	Re_u [1/m]	T_w/T_e [-]
T3A	3	5.4	1.2	$3.60 \cdot 10^5$	1
T3B	6	9.4	1.2	$6.27 \cdot 10^5$	1

The free-stream turbulence level ranges from $Tu_\infty = 3\,\%$ up to $Tu_\infty = 6\,\%$ with very low free-stream velocities u_∞ and $T_w = T_e$, i.e. neither Mach number nor wall temperature effects on turbulent spot growth come into effect. Further, both cases represent experiments on flat plates with zero pressure gradient flow. Based on the experimental results, the measured transition lengths are rather short which suggest that the transition process is mainly driven by the high turbulence level rather than the development of individual turbulent spots. In order to investigate this hypothesis, the spot correction factor is set to $f_\sigma = 1$ which means that the spot production parameter $\hat{n}\sigma$ according to Eq. (10)

only depends on the free-stream turbulence level for the T3 cases. In other words, the Reynolds number effect on turbulent spot growth is neglected using this approach. Regarding the transition onset Reynolds number, the correlation given by Eq. (9) was found to be more suitable for cases with elevated turbulence levels. As it gives the onset Reynolds number based on the momentum thickness, $Re_{\theta t}$ is converted into a corresponding value for Re_{xt} by

$$Re_{xt} = \left(\frac{Re_{\theta t}}{0.664}\right)^2 \tag{17}$$

assuming a Blasius profile. This relation is also used later on to convert between both Reynolds numbers. Further, the laminar and turbulent flow components required to reconstruct a transitional distributions are calculated analytically using classical expressions from boundary layer theory. In particular, the laminar component for the skin friction coefficient $c_{f,lam}$ is obtained from the Blasius solution. Respectively, a classical empirical correlation with $c_{f,turb} = 0.0576\, Re_{xt}^{-1/5}$ is employed for the turbulent counterpart. The resulting skin friction distribution from the linearly-combined transition model for the T3A case is shown in Fig. 5 together with the experimental data as well as the fully laminar and turbulent components.

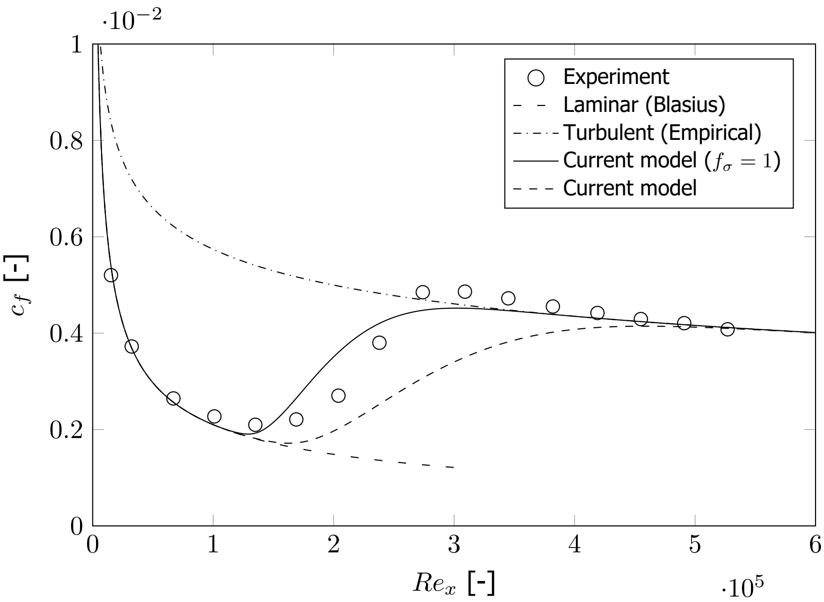

Fig 5. Skin friction coefficient for T3A test case

Using the current transition model, a reasonable description of the transitional zone is obtained for $f_\sigma = 1$ and the transition rate is captured quite well while the transition onset location is predicted a bit too early. If the Reynolds number effect is included, an increased value for the spot trailing edge celerity with $u_{TE} = 0.62\, u_e$ rather than $u_{TE} = 0.39\, u_e$ is found due to the early transition onset at $Re_{\theta t} \approx 200$. This results in a quite low value for the spot growth correction factor with $f_\sigma = 0.32$ and consequently, in a largely extended transition zone as indicated by the dashed line in Fig. 5.

As the current model assumes both laminar and turbulent flow to start from the leading edge of the plate, it is inherently incapable of predicting the overshoot effect. This clearly poses a crucial limitation of the presented linearly-combined model. The results obtained with the current model for the T3B case are given in Fig. 6 and show a reasonable agreement with the experiment if $f_\sigma = 1$ is assumed. Taking the Reynolds number effect on the spot trailing edge celerity u_{TE} into account leads again to a very low transition rate which is not supported by the experimental data. Compared to the T3A case, an earlier onset as well as a shorter transition length due to an elevated free-stream turbulence level is correctly reproduced by the current model.

Given this ambiguity regarding the Re-number effect, a second choice for the constant coefficients c_1 and c_2 in Eq. (10) is considered as it is conceivable that the original coefficients proposed by Mayle [36] already inherently include a Re-number effect. Following the approach that $\hat{n}\sigma Re_{\theta t}^3$ is independent of Tu_∞ according to Narasimha [3], the coefficients are modified to $c_1 = 2.71 \cdot 10^{-11}$ and $c_2 = 2.07$ in order to obtain the same value of $\hat{n}\sigma = 8.55 \cdot 10^{-11}$ found in the T3A case for $f_\sigma = 1$. The corresponding result for the T3B case is given in Fig. 6 and shows very good agreement although the transition rate is slightly lower compared to the case where $f_\sigma = 1$.

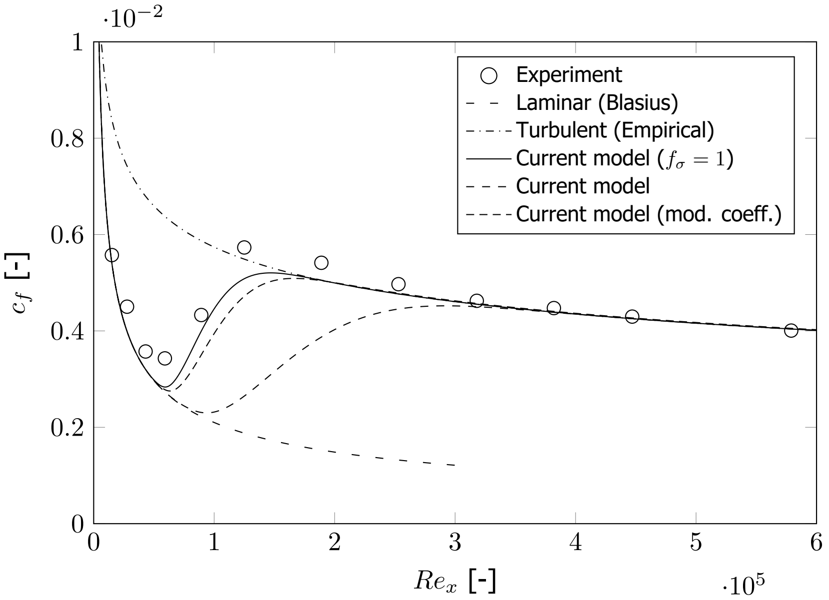

Fig 6. Skin friction coefficient for T3B test case

4.2. RWG-M6 series

Two hypersonic flat plate experiments of the RWG-M6 series, carried out at the Ludwieg-Tube Facility DNW-RWG at DLR Göttingen, were used as validation test cases. A summary of the test conditions is given in Tab. 2 and are taken directly from the experimental report [40].

Table 2. Test conditions of selected RWG-M6 cases

Case	M_e [-]	p_0 [bar]	T_0 [K]	Re_u [1/m]	T_w/T_e [-]
RWG-M6	5.98	12.94	548.8	$9.44 \cdot 10^6$	4.42
RWG-M6-SWBLI	5.98	13.15	511.4	$10.77 \cdot 10^6$	4.74

The RWG-M6 case describes a Mach 6 zero pressure gradient flow without shock impingement. To calculate the laminar and turbulent component of the transitional Stanton number distribution, theoretical expressions are used in this case. In particular, the Chapman-Rubesin approximation in combination with the reference temperature concept by Eckert [41] is used for the laminar distribution whereas an analytical description by White & Christoph [41] is used for the turbulent component.

For the RWG-M6 series no free-stream turbulence levels are explicitly reported, however a value for the Tu_∞ is required within the current transition model to calculate the onset location and transition rate. Therefore, the transition onset correlation from Eq. (8) is solved inversely with the experimental onset Reynolds number and free-stream Mach number which yields a turbulence level of approximately 0.5%. This is slightly below the values given in [19] where 0.6% - 0.7% was estimated for the same case. Further, the transition onset Reynolds number based on the momentum thickness which is needed within the spot growth correlations is calculated as

$$Re_{\theta t} = 0.664\sqrt{Re_{xt}\, C^{\star}} \tag{18}$$

by applying the reference temperature concept to a Blasius profile. The corresponding result of the transition model is shown in Fig. 7 together with experimental data and numerical results obtained with the γ-α model and the Langtry-Menter γ-$Re_{\theta t}$ transition model. For the latter, an extended version according to Krause et al. [43, 44] is employed which is also shown in [19]. Although this extension is particularly designed for hypersonic flow it is clearly not able to correctly reproduce the transition rate and peak Stanton number observed in the experiments. On the other hand, the current transition model seems to capture the transition rate quite well. A crucial limitation of the current model in the given configuration is that it cannot replicate the typical overshoot effect at the end of transition indicated by the experimental data since it is bound between the laminar and turbulent Stanton number distribution. To account for this, the virtual origin of the turbulent flow component could be taken at the transition onset location rather than the leading edge of the plate which was shown in a recent study by Raghunath et al. [45]. However, an attempt like this is not part of the current work as it is difficult to transfer this concept to generic geometries. The γ-α model is able to capture both the peak Stanton number and the transition rate quite well but the transitional overshoot is predicted somewhat further downstream.

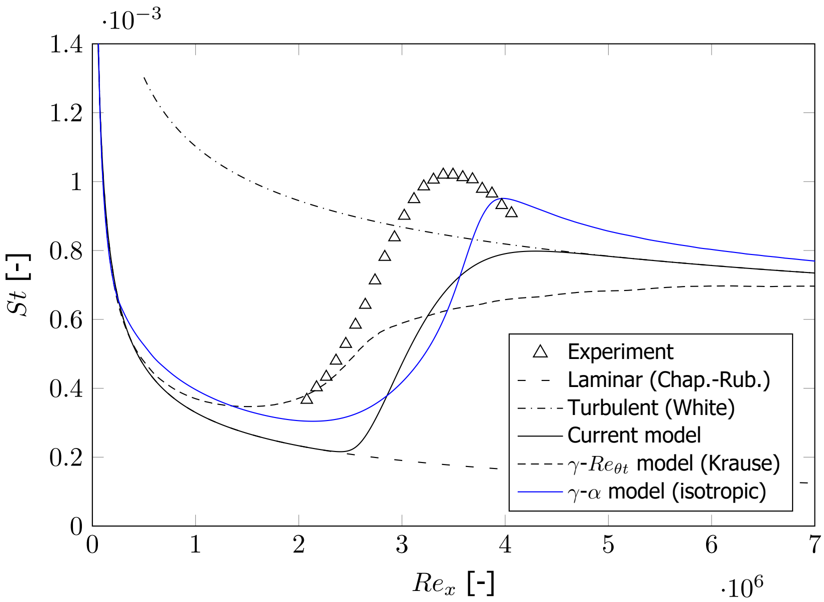

Fig 7. Stanton number distribution for RWG-M6 test case

The second considered test case of the RWG-M6 series includes a shock-wave boundary layer interaction created by an oblique shock wave which impinges the boundary layer near the end of transition. In this case, the laminar and turbulent component for the transitional Stanton number are created with the unstructured CFD solver TAU by Deutsches Zentrum für Luft- und Raumfahrt (DLR) using prismatic cells near the wall and tetrahedral cells otherwise. Regarding the turbulent computation, the classical Menter SST k-ω-model was used as a turbulence model.

Before examining the resulting transitional Stanton number distribution, the impact of the pressure gradient on the intermittency distribution is shown in Fig. 8 based on the laminar CFD solution. It can be inferred that the large adverse pressure gradient found around the impingement location results in a steep increase in the intermittency which immediately yields a fully turbulent flow state that is retained downstream. This is in line with numerical and experimental observations that showed greatly enhanced spot growth for adverse pressure gradients, e.g. [23] or [25].

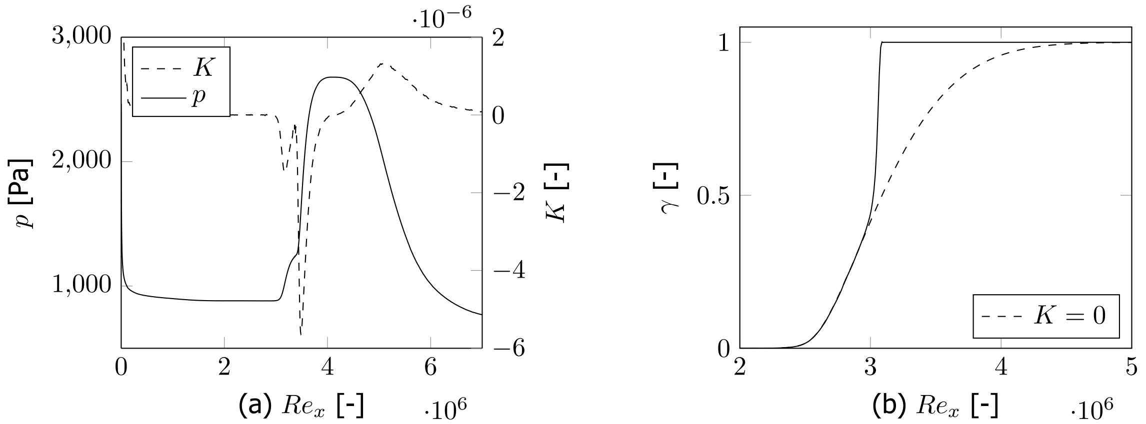

Fig 8. Pressure distribution and pressure gradient parameter (left) and intermittency distribution (right) for RWG-M6-SWBLI case

The corresponding result for the Stanton number distribution is shown in Fig. 9 together with numerical results with the extended γ-$Re_{\theta t}$ transition model and the γ-α model. The same methodology has been applied with respect to Re_{xt}, effectively matching the onset location to the experiment. The plot shows that the peak Stanton number is captured best by the γ-α model followed by the γ-$Re_{\theta t}$ and the current model. Further, unsatisfactory results are obtained with the γ-$Re_{\theta t}$ upstream of the shock impingement location as the onset is predicted too early and the gradual increase of St_{exp} in this region is not reproduced. On the other hand, the current model as well as the γ-α predict the early transition rate much better although the absolute values are still lower compared to the experiment.

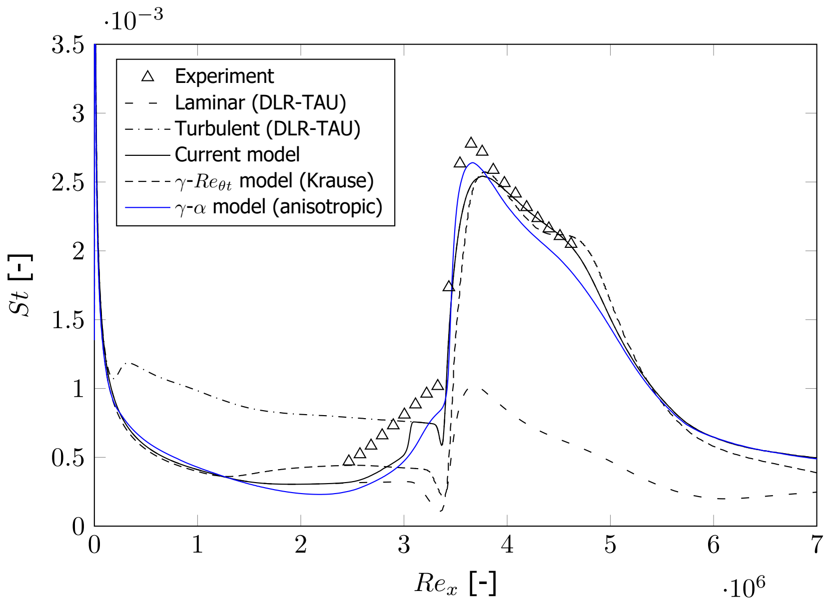

Fig 9. Stanton number distribution for RWG-M6-SBLI case

4.3. ATLLAS-II series

In addition to the RWG-M6 series, the transition model is also applied to two selected test cases that were carried out at the High Enthalpy Shock Tunnel Göttingen (HEG) as part of the ATLLAS-II project[1]. The corresponding test conditions are summarized in Table 2 and are taken from the experimental report [42]. Two flat plate cases with zero pressure gradient flow are considered differing only with respect to their wall temperature condition. While the first case represents a cold wall at $T_w = 295$ K, the wall temperature of the second case is significantly higher with $T_w > 700$ K. Further, the experimental report [42] provides estimates for the spot production parameters with $\hat{n}\sigma_{cold} = 6.66 \cdot 10^{-13}$ and $\hat{n}\sigma_{hot} = 7.78 \cdot 10^{-13}$ which are obtained based on a fit to experimental data. This yields a relative increase between the cold and hot wall of about 17% for the spot production parameter. The current model suggest a lower impact of the wall temperature with a relative increase of about 8%. The resulting Stanton number distributions are given in Fig. 10. The purely laminar and turbulent flow components for the reconstruction of the transitional Stanton number are determined using the same analytical expressions from boundary layer theory as in the RWG-M6 case.

Table 3. Test conditions of selected ATLLAS-II cases

Case	M_e [-]	p_0 [bar]	T_0 [K]	Re_u [1/m]	T_w/T_e [-]
Cold wall	7.4	31.54	2687	$6.65 \cdot 10^6$	1.13
Hot wall	7.4	31.54	2687	$6.65 \cdot 10^6$	2.68

Again values the free-stream turbulence level are not directly available, however an estimate of 0.6% is given in the experimental report which is adopted within the current work. Further, it is important to mention that the onset Reynolds number Re_{xt} is chosen to match with the experimental onset point for both cases. The onset correlation from Eq. (8) predicts an early transition with $Re_{xt} = 1.46 \cdot 10^6$ for both cases as the effect of wall temperature is not included. Incorporating this effect is quite complex because it depends on the prevalent instability mode and thus, is not easily reproducible within a simple correlation.

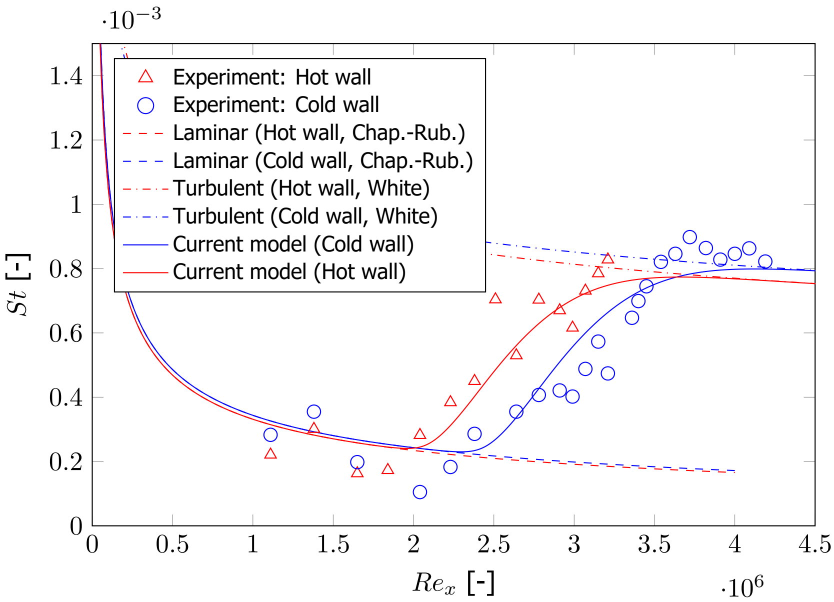

Fig 10. Stanton number distribution for ATLLAS-II test cases

[1]https://www.esa.int/Enabling_Support/Space_Engineering_Technology/ATLLAS_II_-_Project_summary

In this case, the experimental Stanton number distributions indicate an earlier start of transition for the hot wall case. The current transition model is able to reproduce the experimentally measured Stanton number distributions reasonably well although it is difficult to infer the impact of the wall temperature on the transition rate using this representation.

5. Application to hypersonic flight vehicle

A boundary layer tool developed by Hoffmann et al. [46] has been extended as part of this work by means of implementing the currently proposed linearly-combined transition model. In particular, the tool provides distance approximations of surface streamlines from an attachment line and in addition, variables at the local boundary layer edge based on a three-dimensional flow field input. By assuming that the near-wall intermittency distribution given by Eq. (7) develops along the surface streamline coordinate s, a description of the intermittency distribution can be obtained *a posteriori* with the current transition model. A detailed description of the streamline length calculation algorithm is provided in [46]. An example of this application is given in Fig. 11 where field data of a laminar three-dimensional flow simulation generated by the DLR-TAU code is used as tool input.

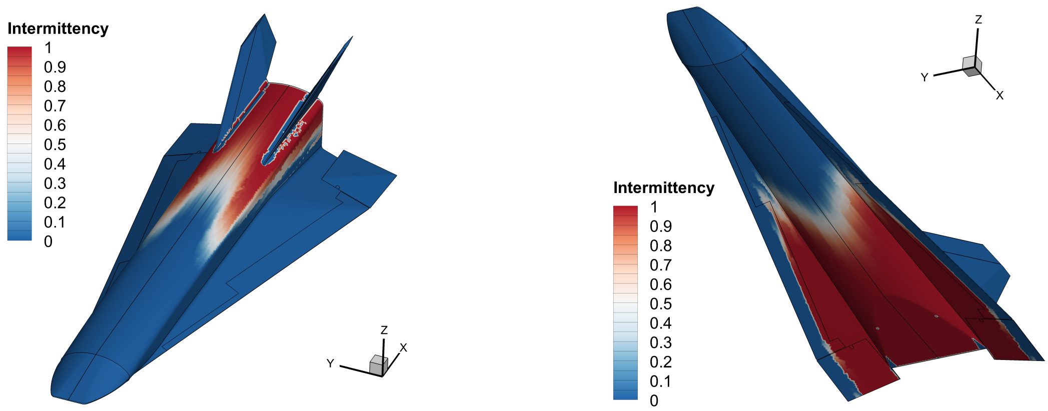

Fig 11. Intermittency distribution on leeward (left) and windward side (right) of EFTV

The geometry represents the European Flight Test Vehicle (EFTV) - a hypersonic glider model which has been designed in the framework of the HEXAFLY-INT project[2] coordinated by the European Space Agency. It will be tested in a free-flight scenario where a hypersonic cruise phase at Mach 7 is planned [47]. The setup of the considered purely laminar flow simulation is given in Table 4 and aims to replicate a particular point along the scheduled trajectory, approximately 309.55 s after release from the launcher.

Table 4. EFTV simulation conditions

Case	$Altitude$ [m]	M_e [-]	Re_u [1/m]	AoA [°]
243-01	$28\,040$	7.03	$3.73 \cdot 10^6$	1.63

To calculate the transition onset location, a correlation proposed by Bowcutt et al. [48] is used

$$\log_{10}(Re_{xt}) = 6.421 \exp(1.209 \cdot 10^{-4} M_e^{2.641}) \tag{19}$$

[2]https://www.esa.int/Enabling_Support/Space_Engineering_Technology/High-Speed_Experimental_Fly_Vehicles_-_INTernational

which relates the transition onset Reynolds number to the Mach number at the boundary layer edge. However, the tool offers the flexibility to choose from different onset correlations depending on the given configuration. Using the current setup, the tool predicts transitional regions on both sides of the vehicle body starting around midway along the surface. Further, no transitional regions are found on the leeward side of the wings. This is generally in line with results given [47] where a transition assessment for the same geometry was carried out.

6. Conclusion

In the current work, a simplified transition model was presented that uses an empirically calculated intermittency distribution to describe the transitional region. It does not involve solving a system of partial differential equations but rather blends purely laminar and turbulent solutions *a posteriori* by means of a linear combination using the intermittency as a weighting factor. The mechanisms of turbulent spot growth are incorporated by means of an empirical model which has been derived based on spot growth data from literature. Partly due to different measurement techniques and spot shape definitions, a reasonable collapse of the available data is currently not possible. Conventions regarding these aspects are required to enable a generic comparison of the data within future turbulent spot studies.

In its current version, the proposed transition model is able to capture reasonably well compressibility, Reynolds number, temperature and also pressure gradient effects on the transition rate. It has been validated for a number of test cases including zero and non-zero pressure gradient flow and generally showed reasonable agreement with experimental data. However, a crucial limitation of the current model is its inability to predict the overshoot effect at the end of transition as it always is bound between the fully laminar and turbulent distributions.

The transition model was further applied to a full vehicle by implementing it into a previously developed boundary layer analysis tool. This allows to use best-practice correlations to obtain an approximative description of the transition zone on generic geometries. The results could be considered in the context of an initial assessment of aero-thermal loads during the design phase of high-speed vehicles. However, in order to explore the full potential of this extended transition tool it certainly has to be validated for a number of test cases in a future work.

References

[1] A. Whitehead, Jr.: NASP aerodynamics. AIAA Paper 89-5013, 1989.

[2] Defense Science Board: Report of the Defense Science Board task force on the National Aerospace Plane (NASP). DTIC citation AD-A201124, 1988.

[3] Narasimha, R.: The laminar-turbulent transition zone in the boundary layer. Progress in Aerospace Sciences, 22(1), pp.29-80, 1985.

[4] Narasimha, R., & Dey, J.: Transition-zone models for 2-dimensional boundary layers: A review. Sadhana, 14(2), 93-120, 1989.

[5] Emmons H. W.: The laminar-turbulent transition in a boundary layer—Part I. Journal of the Aeronautical Sciences 490–8, 1951.

[6] Dhawan, S. J., & Narasimha, R.: Some properties of boundary layer flow during the transition from laminar to turbulent motion. Journal of Fluid Mechanics, 3(4), 418-436, 1958.

[7] Solomon, W. J., G. J. Walker, and J. P. Gostelow.: Transition length prediction for flows with rapidly changing pressure gradients. ASME 1995 International Gas Turbine and Aeroengine Congress and Exposition, American Society of Mechanical Engineers Digital Collection, 1995.

[8] Chen, K. K., & Thyson, N. A.: Extension of Emmons' spot theory to flows on blunt bodies. AIAA Journal, 9(5), 821-825, 1971.

[9] Adams Jr, J. C.: Numerical calculation of sharp flat plate transitional and turbulent skin friction. AIAA Journal 10.6, 841-843, 1972.

[10] Cebeci, T., & Smith, A. M. O.: Analysis of Turbulent Boundary Layers, Academic Press, 1974.

[11] Steelant, J. & Dick, E.: Modelling of Bypass Transition with Conditioned Navier-Stokes Equations Coupled to an Intermittency Transport Equation. International Journal for Numerical Methods in Fluids, Vol. 23, pp. 193–220, 1996.

[12] Steelant, J. & Dick, E.: Prediction of By-Pass Transition by Means of a Turbulence Weighting Factor - Part I : Theory and Validation. ASME paper 99-GT-29, 1999.

[13] Steelant, J. & Dick, E.: Prediction of By-Pass Transition by Means of a Turbulence Weighting Factor - Part II: Application on Turbine Cascades," ASME paper 99-GT-30, ASME, 1999.

[14] Simon, F. F., & Stephens, C. A.: Modeling of the heat transfer in bypass transitional boundary-layer flows. NASA Technical paper 3170, 1-12, 1991.

[15] Suzen, Y. B. & Huang, P. G.: Modeling of flow transition using an intermittency transport equation. Journal of Fluids Engineering, Vol. 122, No. 2, pp. 273–284, 2000.

[16] Cho, J. R. & Chung, M. K.: A K-ϵ-γ equation turbulence model. Journal of Fluid Mechanics, Vol. 237, p. 301, 1992.

[17] Menter, F. R., Langtry, R. B., Likki, S. R., Suzen, Y. B., Huang, P. G., and Völker, S.: A Correlation-based Transition Model Using Local Variables - Part I: Model Formulation. Journal of Turbomachinery, Vol. 128, No. July 2006, 2006.

[18] Langtry, R. B., Menter, F. R., Likki, S. R., Suzen, Y. B., Huang, P. G., & Völker, S.: A Correlation-Based Transition Model Using Local Variables - Part II: Test Cases and Industrial Applications. Journal of Turbomachinery, Vol. 128, No. 3, p. 423, 2006.

[19] Van den Eynde, J. & Steelant, J.: Two-Equation Transition Model Based on Intermittency and Empirical Correlations. International Conference on High-Speed Vehicle Science Technology, 2018.

[20] Van den Eynde, J., Steelant, J., and Passaro, A.: Intermittency-based Transition Model with Local Empirical Correlations. 21st AIAA International Space Planes and Hypersonics Technologies Conference, pp. 1–16, 2017.

[21] Narashimha, R.: On the distribution of intermittence in the transition region of a boundary layer. Journal of Aeronautical Science 24: 711-712, 1957.

[22] Wygnanski I, Zilberman M, Haritonidis J. H.: On the spreading of a turbulent spot in the absence of a pressure gradient. Journal of Fluid Mechanics 123, 69-90, 1982.

[23] Johnson, M. W.: Prediction of turbulent spot growth rates. ASME 1999 International Gas Turbine and Aeroengine Congress and Exhibition. American Society of Mechanical Engineers Digital Collection, 1999.

[24] Katz, Y., Seifert, A. & Wygnanski, I.: On the evolution of the turbulent spot in a laminar boundary layer with a favourable pressure gradient. Journal of fluid mechanics 221 pp. 1-22, 1990.

[25] Seifert, A. & Wygnanski, I.: On turbulent spots in a laminar boundary layer subjected to a self-similar adverse pressure gradient. Journal of Fluid Mechanics, 296, pp.185-209, 1995.

[26] Clark, J. P., Jones, T. V. & LaGraff, J. E.: On the propagation of naturally-occurring turbulent spots. J. Engng Maths 28, 1–19, 1994.

[27] Van den Eynde, J. & Steelant, J.: Compressibility and temperature effects on turbulent spot growth. International Conference on High-Speed Vehicle Science Technology, 2018.

[28] Fischer, M. C.: Spreading of a turbulent disturbance. AIAA J. 10(7), 1972.

[29] Chong, T. P & Zhong, S.: On the Three-Dimensional Structure of Turbulent Spots. Journal of Turbomachinery, Vol. 127, No. 3, p. 545, 2005.

[30] Gad-El-Hak, M., Blackwelderf, R.F. & Riley, J.J.: On the growth of turbulent regions in laminar boundary layers. Journal of Fluid Mechanics, 110, pp.73-95, 1981.

[31] Redford, J. A., Sandham, N. D., & Roberts, G. T.: Numerical simulations of turbulent spots in supersonic boundary layers: Effects of Mach number and wall temperature Progress in Aerospace Sciences, Vol. 52, pp. 67–79, 2012.

[32] Sandham, N.D.: Effects of compressibility and shock-wave interactions on turbulent shear flows. Flow, Turbulence and Combustion, 97(1), pp.1-25, 2016.

[33] Jocksch, A. and Kleiser, L.: Growth of turbulent spots in high-speed boundary layers on a flat plate. International Journal of Heat and Fluid Flow, 29(6), pp.1543-1557, 2008.

[34] Schubauer, G. B. & Klebanoff, P. S.: Contributions on the mechanics of boundary layer transition. NACA TN 3489, 1955.

[35] Doorly, D. J. & Smith, F. T.: Initial-value problems for spot disturbances in incompressible or compressible boundary layers. Journal of Engineering Mathematics, Vol. 26, No. 1, pp. 87–106, 1992.

[36] Mayle, R. E.: The Role of Laminar-Turbulent Transition in Gas Turbine Engines. Journal of Turbomachinery, Vol. 113 pp. 509-536, 1991.

[37] Vinod, N and Govindarajan, R.: Pattern of breakdown of laminar flow into turbulent spots, Physical review letters, V. 93, No. 11, pp. 1-4, 2004.

[38] Steelant, J., & Dick, E.: Modeling of laminar-turbulent transition for high freestream turbulence. J. Fluids Eng., 123(1), 22-30, 2001.

[39] Roach, P. E. & Brierley, D. H.: The Influence of a Turbulent Free-Stream on Zero Pressure Gradient Transitional Boundary layer Development Including the T3A and T3B Test Case Conditions, Proc. 1st ERCOFTAC Workshop on Numerical Simulation of Unsteady Flows, Transition to Turbulence and Combustion, 1990.

[40] Schülein, E. : Effects of laminar-turbulent transition on the shock-wave/boundary-layer interaction, 44th AIAA Fluid Dynamics Conference, 2014.

[41] White, F. M.: Viscous fluid flow, Vol. 3. McGraw-Hill, 2006.

[42] Wagner, A. & Benjamin, L.: Shock Waves Boundary Layer Interaction at Varying Model Surface Temperatures in the High Enthalpy Shock Tunnel Göttingen, Del. No. D5.1.4, 2019

[43] Krause, M., Behr, M., and Ballmann, J.: Modeling of Transition Effects in Hypersonic Intake Flows Using a Correlation-Based Intermittency Model," 15th AIAA International Space Planes and Hypersonic Systems and Technologies Conference, American Institute of Aeronautics and Astronautics, Reston, Virigina, pp. 1–12., 2008.

[44] Krause, M.: Numerical analysis of transition effects for SCRamjet intake flows. Ph.D. thesis, RWTH Aachen, 2010.

[45] Raghunath, S., Mee, D. and Narasimha, R.: Estimating turbulent spot initiation rates from transition lengths in hypersonic boundary layers. AIAA Journal, pp.3640-3647, 2017.

[46] Hoffmann, P., Van den Eynde, J., Steelant, J.: Boundary Layer and Transition Onset Assessment on Generic Geometries. International Conference on High-Speed Vehicle Science Technology, 2020.

[47] Steelant, J., Passaro, A., Villace, V.F., Gubanov, A., Ivanyushkin, D., Shvalev, Y., Voevodenko, N., Marini M., Di Benedetto, S.: Boundary Layer Transition Assessment on a Slender High-Speed Vehicle. 21st AIAA International Space Planes and Hypersonics Technologies Conference, 2017.

[48] Bowcutt, K.G., Anderson, J.D., Capriotti, D.: Viscous Optimized Hypersonic Waveriders. AIAA 25th Aerospace Science Meeting, 1987.

[49] Fiala, A., Hillier, R., Mallinson, S. G., & Wijesinghe, H. S.: Heat transfer measurement of turbulent spots in a hypersonic blunt-body boundary layer. Journal of Fluid Mechanics, 555, pp.81-111., 2006.

[50] Sivasubramanian, J., and Fasel, H. F.: Direct numerical simulation of a turbulent spot in a cone boundary layer at Mach 6. 40th Fluid Dynamics Conference and Exhibit, 2010.

[51] Mee, D. J: Boundary-Layer Transition Measurements in Hypervelocity Flows in a Shock Tunnel. AIAA Journal, Vol. 40, No. 8, pp. 1542–1548, 2002.